

Titanium ditelluride: Band structure, photoemission, and electrical and magnetic properties

D. K. G. de Boer, C. F. van Bruggen, G. W. Bus, R. Coehoorn, C. Haas, and G. A. Sawatzky
*Laboratories of Inorganic and Physical Chemistry, Materials Science Center of the University,
 Nijenborgh 16, 9747-AG Groningen, The Netherlands*

H. W. Myron

Laboratory for High Magnetic Fields, University of Nijmegen, Toernooiveld, 6225-ED Nijmegen, The Netherlands

D. Norman and H. Padmore

Daresbury Laboratory, Science and Engineering Research Council, Daresbury, Warrington WA4 4AD, United Kingdom

(Received 26 September 1983)

We present a study of angle-resolved photoemission of the layered compound TiTe_2 . The results are compared to augmented-plane-wave band-structure calculations which predict TiTe_2 to be a semimetal with an overlap of valence and conduction bands of 0.6 eV. Reasonable agreement with the calculations is found except for an almost dispersionless band found just below the Fermi level which is not present in the theory. This band is argued to result from either a narrow impurity band or localization of electrons due to the formation of polarons. From an analysis of resistivity, thermoelectric power, and Hall effect, we deduced the carrier concentrations and mobilities for $\text{Ti}_{1.01}\text{Te}_2$. The large value of the Pauli susceptibility indicates large exchange enhancement. At 150 K, a phase transition was detected in magnetic susceptibility measurements. The corresponding lattice distortion could not be observed directly.

I. INTRODUCTION

TiTe_2 belongs to the class of transition-metal dichalcogenides with a layered structure. Because of their pseudo-two-dimensional nature, the physics and chemistry of these materials are of interest. For instance, many of them show phase transitions to a modulated crystal structure, often referred to as a charge-density wave.¹ At the transition the electron structure also changes, having a repercussion on the physical properties.

The layered compounds TiS_2 and TiSe_2 have been especially widely studied. Stoichiometric TiS_2 without atomic disorder is believed to be a semiconductor with an indirect gap of a few tenths of an electron volt. However, all investigated TiS_2 materials with approximately the right stoichiometry are metallic, which, according to Wilson, is due to electrons in an impurity band.² Angle-resolved ultraviolet photoelectron spectroscopy³⁻⁵ (ARUPS) indicates occupation of states at the Fermi level mainly at the $M(L)$ point in \vec{k} space, where a gap with the sulfur bands is seen.

TiSe_2 is a semimetal displaying a periodic lattice distortion below 200 K.⁶ ARUPS (Refs. 3 and 7-9) indicates a small band overlap. Below the transition temperature the Ti d emission sharpens at the $M(L)$ point, indicating the enhancement of the density of states just below E_F .^{10,11} The difference in nature of the valence and conduction bands in TiS_2 and TiSe_2 is confirmed by pressure-dependent Hall measurements^{12,13} and also by self-consistent band-structure calculations.¹⁴

As is expected, TiTe_2 is a semimetal with a still larger band overlap than TiSe_2 . After a short discussion of the crystal structure (Sec. III) we present an electronic band-

structure calculation for this material (Sec. IV). In Sec. V our ARUPS measurements are compared with the calculated band structure, and then (Sec. VI) our magnetic and transport measurements are discussed.

One of the most interesting aspects of this work is that, with ARUPS, a state is found just below the Fermi level in which different wave vectors are involved. We suggest that localization of electrons by (vibronic or electronic) polarization of the environment is responsible for this.

II. EXPERIMENTAL

TiTe_2 powder was obtained by heating nearly stoichiometric amounts of the elements (with a slight excess of Te) at 750°C. Single crystals were prepared from this powder by iodine-vapor transport (800→700°C). Chemical analysis showed the presence of 1 at. % excess Ti. The crystals are hexagonal platelets with a metallic luster and characteristic dimensions of $5 \times 5 \times 0.1 \text{ mm}^3$.

For the ARUPS measurements the crystal was glued on to a sample holder with silver-bearing resin. In order to obtain a fresh surface, the crystal was stripped in the preparation chamber attached to the spectrometer at a pressure below 10^{-6} Pa. Immediately thereafter, the sample was transferred into the ultrahigh-vacuum main chamber (base pressure better than 10^{-8} Pa). The spectrometer used is a Vacuum Generators model no. ADES 400. The polar angle of incidence of the light α and the polar angle of emission of the electrons θ can be selected, as is shown schematically in Fig. 1. The azimuth φ can also be varied. The spread in the detected emission angle is estimated to be $\pm 2^\circ$. Unpolarized light is obtained from a helium-gas-discharge lamp, supplying

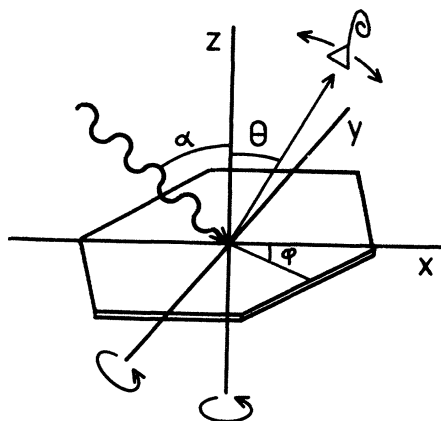


FIG. 1. Experimental geometry for angle-resolved photoemission. The crystal surface coincides with the x - y plane. In the x - y plane the light has an angle of incidence α and the electrons are detected at the emission angle θ . By varying φ the emission plane can be selected.

light of 21.2 (He I) and of 40.8 eV (He II). Polarized light at energies between 40 and 70 eV was obtained from the Daresbury Laboratory synchrotron (Daresbury, United Kingdom) using a grazing-incidence monochromator. The analyzer was used with a constant pass energy, which was set mostly at 5 eV for light with $\hbar\omega = 21.2$ eV, and at 20 eV for $\hbar\omega$ above 40 eV. The energy resolution is 2–2.5% of the pass energy.

The x-ray photoelectron spectrum of Fig. 4 of a polycrystalline sample which was scraped in the preparation chamber attached to the spectrometer, was taken with an AEI ES 200 spectrometer. In this way both a carbon- and oxygen-free sample was obtained. Our spectrum is in reasonable agreement with that published by Arnaud,¹⁵ although the latter is broadened to higher binding energy, a characteristic probably due to contamination with oxygen.

The magnetic susceptibility of nonoriented crystals was measured with the Faraday method at $H = 8.76$ kOe. The Hall effect of a TiTe_2 crystal plate was measured with a double-ac technique, and the in-plane resistivity of the same crystal was measured with the four-contact method. The thermoelectric power of a polycrystalline sample was measured with respect to gold contacts.

III. CRYSTAL STRUCTURE

Like many of the early transition-metal dichalcogenides, TiTe_2 adopts the $1T$ - CdI_2 structure, which has a hexagonal close packing of anions with the metal atoms in octahedral holes. The space group for this structure is $P\bar{3}m1$ (D_{3d}^3). In Fig. 2 we show a projection of the structure on the xy plane and a (110) section, by which their structures are easily represented, as these sections contain all atoms. We also show the reciprocal lattice and the Brillouin zone for this structure. Each metal atom is surrounded by a trigonally distorted octahedron of anions; the trigonal distortion depends on the z parameter of the structure [Fig. 2(b)].

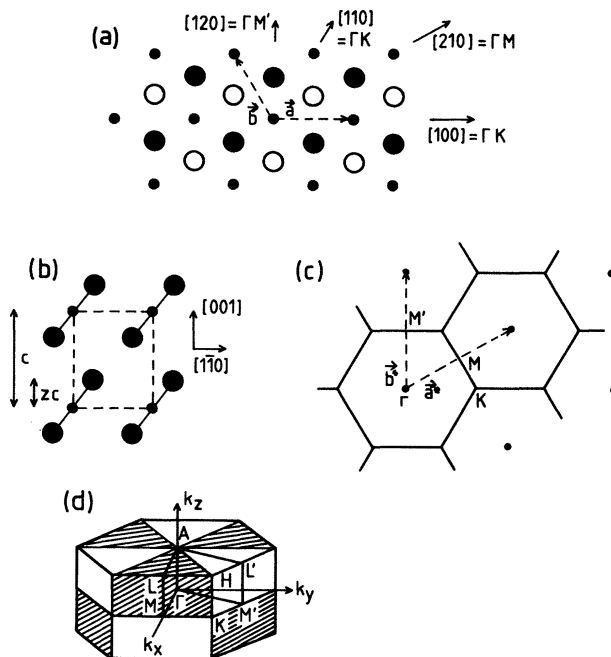


FIG. 2. (a) Projection of the CdI_2 structure on the x - y plane. Small solid circles represent cations in the plane, large open circles are anions under the plane, and large solid circles are anions above the plane. Some directions of high symmetry are indicated. (b) (110) section of the CdI_2 structure. (c) Reciprocal lattice of the CdI_2 structure in the k_x - k_y plane. The Brillouin zone is shown in the repeated-zone representation. (d) Brillouin zone of the CdI_2 structure. One of the 12 irreducible wedges is shown by heavy solid lines. Although the surfaces of the shaded and unshaded wedges are equivalent by symmetry, their interiors are not.

The lattice parameters are¹⁵ $a = 3.777$ Å, $c = 6.498$ Å, and $z = 0.2628$, resulting in strongly trigonally stretched TiTe_6 octahedron (top angle = 86°). The crystal axes we found are in close agreement with these data. X-ray and electron diffraction (Rijksuniversitair Centrum Antwerpen, Antwerp, Belgium) revealed no lattice distortion between 300 and 100 K,¹⁶ indicating that the distortions suggested by anomalies in the magnetic and transport data (Sec. VI) are small or local in character.

The six M points in the Brillouin zone cannot be distinguished, but there are two different ΓM directions which we will designate ΓM and $\Gamma M'$. These are defined as follows: In going from a metal atom in the ΓM direction the first-neighbor ligand lies under the ΓM line, whereas in the $\Gamma M'$ direction the first-neighbor ligand lies above the $\Gamma M'$ line. To distinguish the two directions in the ARUPS measurements we performed Laue x-ray backreflection.

IV. BAND-STRUCTURE CALCULATION OF TiTe_2

Early band-structure calculations of TiTe_2 were performed by Murray¹⁷ using a semiempirical LCAO method, and by Bullett¹⁸ with an *ab initio* LCAO method. In the first calculation several crude approximations were

made, whereas Bullett¹⁸ used a limited basis set and did not take into account Te 5*d* levels. A more serious shortcoming of these calculations is that they do not use the correct *z* parameter of the Te atoms [see Fig. 2(b)], yielding an incorrect trigonal distortion of the octahedra of Te atoms surrounding Ti. The position of the Ti 3*d*₂-derived band is especially sensitive for the trigonal distortion. Furthermore in none of these works is calculated the position of the Fermi level.

In this section we present augmented-plane-wave (APW) calculations of TiTe₂ by Myron.¹⁹ The method used is described elsewhere.^{20,21} The muffin-tin radii for both Ti and Te were 1.086 Å. The crystal potential was calculated from the atomic configurations Ti 3*d*³4*s*¹ and Te 5*s*²5*p*⁴. Relativistic effects such as spin-orbit coupling were not taken into account. The local approximation for exchange (*Xα*) was used.

The energies were first calculated in a limited number of points in reciprocal-lattice space for the values 0.7 and 1.0 of the exchange parameter *α*. Some of the calculated values are presented in Table I. The calculations were compared with the measured photoelectron spectra. Although the energies for both values of *α* agree reasonably well with experiment, the agreement for *α*=1.0 is somewhat better. First, the width of the occupied part of the Te 5*p*-derived bands determined by x-ray photoelectron spectroscopy (XPS) is about 5.5 eV, whereas the calculated values of the width of the occupied part of the bands are 5.9 and about 6.3 eV for *α*=1.0 and 0.7, respectively. In ARUPS we could unambiguously identify the Ti 3*d*-derived band (*M*₁⁺, *L*₁⁺) just below *E_F* and a Te 5*p*- and Ti 3*d*-derived band (*M*₂⁺, *L*₂⁺) at a distance of 2.0 eV. The distances calculated with *α*=0.7 and 1.0 are 1.7 and 2.0 eV, respectively. Finally, the position

TABLE I. Widths of the Te 5*s* - and Te 5*p* -, Se 4*s* - and Se 4*p* -, and S 3*s* - and S 3*p* - derived bands, *s-p* gap, and gap between chalcogen *p*- and metal *d*-derived bands (denoted by an asterisk superscript) in titanium dichalcogenides. All values are in eV. The values for TiSe₂ and TiS₂ were tabulated by Zunger (Ref. 22).

	TiTe ₂ <i>α</i> =1.0	TiTe ₂ <i>α</i> =0.7	TiSe ₂ ^a	TiS ₂ ^b
Width of <i>s</i> band	2.45	2.72	2.00	1.94
Width of <i>p</i> band	6.26	6.80	5.70	5.49
<i>s-p</i> gap	4.00	3.40	6.92	6.76
<i>p-d</i> gaps: $\Gamma\Gamma^*$	0.11	0.00	0.32	0.84
MM^*	1.96	1.61	2.04	2.51
LL^*	1.12	0.75	1.32	1.63
ΓM^*	-0.33	-0.91	0.12	0.29
ΓL^*	-0.63	-1.22	-0.20	0.23
Edge of <i>p</i> band	Γ_3^-	Γ_2^-	Γ_3^-	Γ_2^-

^aReference 14(b).

^bReference 14(a).

of the Te 5*s* band is predicted a little more accurately with *α*=1.0. Therefore it was decided to calculate the full band structure with *α*=1.0.

The energy bands along high-symmetry directions are shown in Fig. 3. The density of states derived from the band structure depicted in Fig. 3 is shown in Fig. 4. The Fermi level is 8.4 eV above the muffin-tin zero of energy. The Te 5*p*-derived bands extend from 5.85 eV below *E_F* up to 0.41 eV above *E_F*. The Ti 3*d*-derived bands begin at 0.22 eV below *E_F* in a *L*₁⁺ state. Here, qualitatively the same features are found as in previous calculations for transition-metal dichalcogenides with the same structure. The calculations by Zunger and Freeman^{14,22} give the best

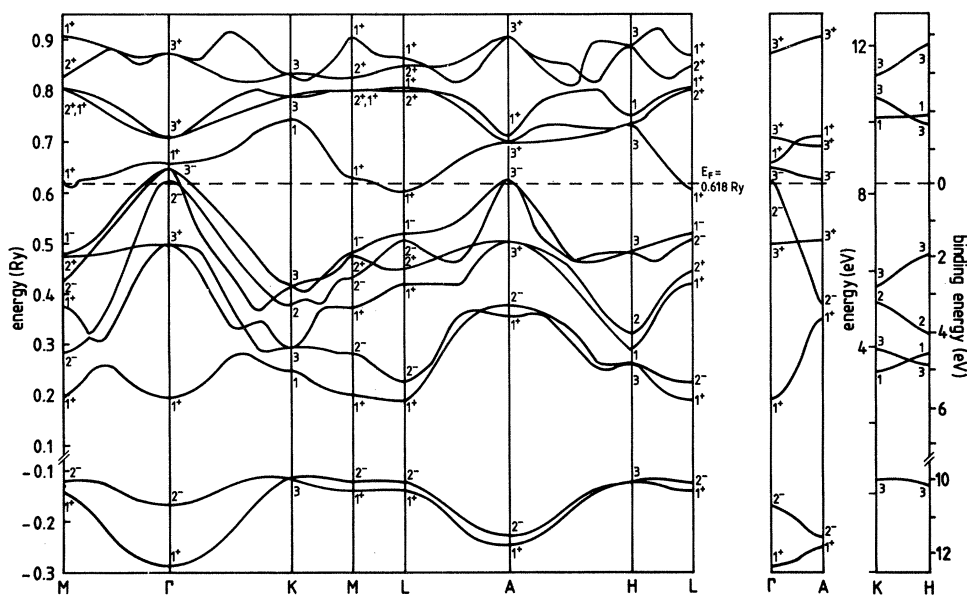


FIG. 3. Electronic band structure of TiTe₂ calculated along lines of high symmetry with the APW method (*α*=1). At the right the binding energy with respect to *E_F* is given. The other energies are with respect to the muffin-tin zero.

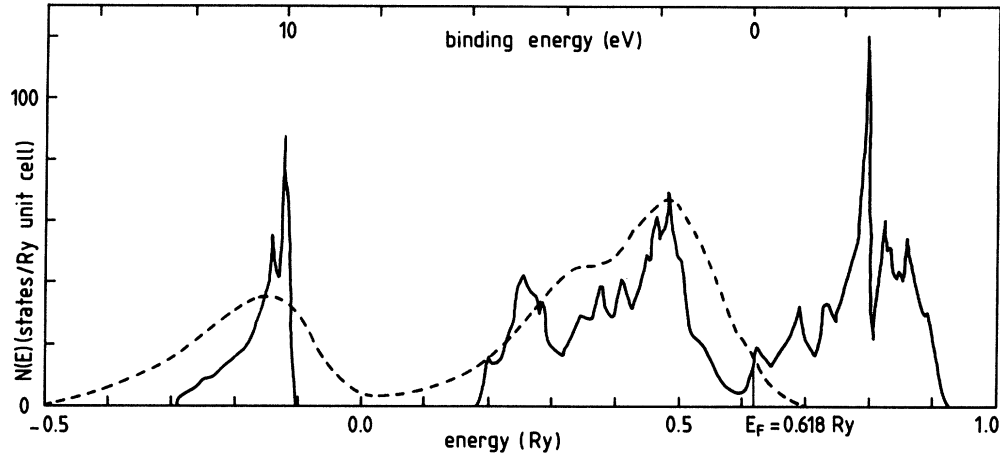


FIG. 4. Electronic density of states for TiTe_2 calculated from the band structure of Fig. 3. The valence-band spectrum measured with XPS is shown as a dashed line.

agreement with experiment. In Table I we included values from their calculations for TiSe_2 and TiS_2 . As expected, the chalcogen p -derived band becomes broader and the gaps become smaller (or the overlap larger) in the series TiS_2 , TiSe_2 , and TiTe_2 . No analysis of the nature of the wave functions of TiTe_2 was carried out. When needed, we will use the wave functions calculated for the compound CrSe_2 ,¹⁹ which has the same crystal structure as TiTe_2 as well as a similar band structure.

Next we discuss the splitting of Ti $3d$ -derived bands at Γ . From crystal-field theory one expects the metal d levels to split in an octahedral surrounding of anions into t_{2g} and e_g levels. Indeed, in compounds with the $1T\text{-CdI}_2$ structure with perfectly octahedral coordination, the d_{z^2} -derived level (Γ_1^+) coincides with one of the Γ_3^+ doublets. In TiTe_2 , as in VSe_2 ,^{21,22} the metal atom resides in a strongly trigonally elongated octahedron, causing the Γ_1^+ state to split off. However, t_{2g} -derived Γ_3^+ states turn out to be antibonding, an effect for which nearest-neighbor interactions alone cannot account.

In Fig. 5 the Fermi surface of TiTe_2 calculated from the band structure of Fig. 3 in planes of high symmetry is

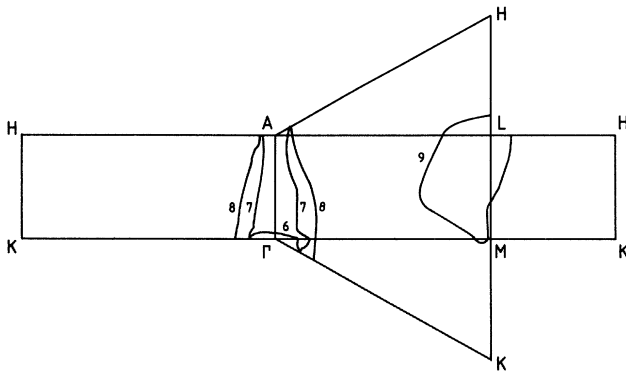


FIG. 5. Fermi surface of TiTe_2 calculated from the band structure of Fig. 3 along planes of high symmetry.

shown. There are four bands which intersect the Fermi level. The four surfaces are numbered in Fig. 5 in the order in which the corresponding bands occur near point Γ . There is an electron surface round point L (sheet 9), a small hole surface around point Γ (sheet 6), and two nearly cylindrical hole surfaces along line ΓA (sheets 7 and 8). Note that around point M the surface⁹ is also holelike. The volume enclosed by the surface yields the number of charge carriers available for conduction. Through integration we found that there are 9×10^{-4} holes in sheet 6, 1.33×10^{-2} holes in sheet 7, and 3.76×10^{-2} holes in sheet 8, adding up to 0.052 holes per unit cell. Thus, sheet 9, which is difficult to integrate, must contain 0.052 electrons. For $\alpha=0.7$ the band overlap is about twice that for $\alpha=1.0$. We estimate that for $\alpha=0.7$ the number of charge carriers is a few tenths per Ti atom.

V. ANGLE-RESOLVED PHOTOEMISSION OF TiTe_2

Figures 6–8 display some of the photoelectron spectra which we measured in the ΓM and ΓK directions with He I and He II radiation. For all of these spectra the angle of incidence of the light is 45° . For other angles of incidence the same peaks are seen, but the intensities are different. Furthermore, in the ΓM and $\Gamma M'$ directions (see Fig. 2), the same peak positions are obtained, although the intensities can differ. In Fig. 9 we show spectra taken at normal emission with synchrotron radiation of different photon energies and polarization directions.

A. Determination of the band structure

To obtain information on the band structure from the angle-resolved photoemission spectra we follow the work of Mahan²³ and Hughes.²⁴ If the direction of the outgoing electron makes the angle θ with the normal on the surface of the solid, the component of its wave vector parallel to the surface is

$$k_{\parallel} = [(2m/\hbar^2)(\hbar\omega - \Phi - E_b)]^{1/2} \sin\theta,$$

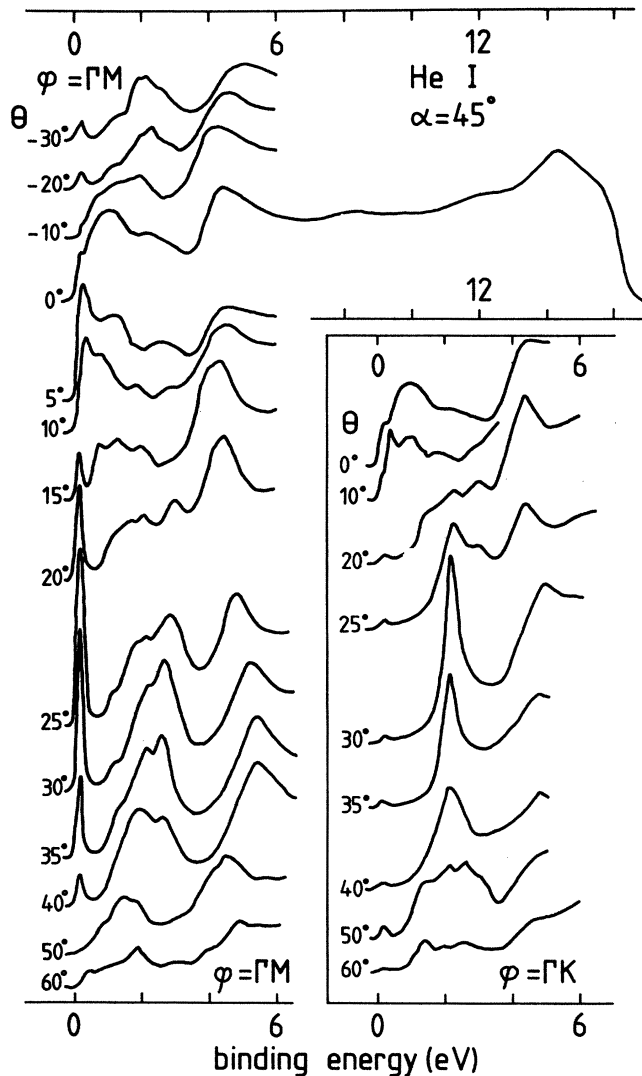


FIG. 6. HeI photoelectron spectra of TiTe_2 in the ΓMA plane (left) and the ΓKA plane (right) for various emission angles θ , with angles of incidence $\alpha = 45^\circ$. Note that for the spectra at the right the background is higher.

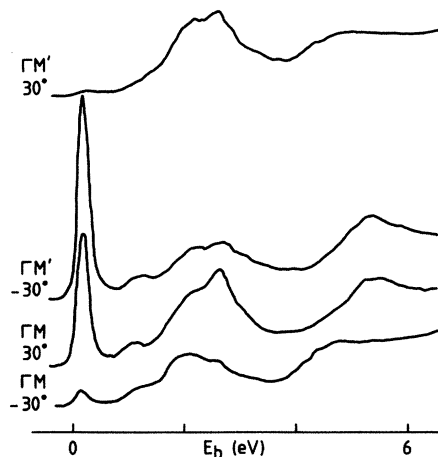


FIG. 7. HeI photoelectron spectra of TiTe_2 in the ΓMA and the $\Gamma M'A$ plane for $\theta = \pm 30^\circ$ and $\alpha = 45^\circ$. Note that $\theta = -30^\circ$ for $\varphi = \Gamma M$ corresponds to emission in the $\Gamma M'$ direction.

where $\hbar\omega$ is the photon energy, Φ is the work function, and E_b is the ionization potential with respect to the Fermi level (E_F), often referred to as the binding energy. This \vec{k}_{\parallel} is equal to the initial parallel wave vector in the repeated-zone scheme. To obtain the perpendicular component k_{\perp} we have to know the dispersion for the final state inside the solid. Approximating this by a free-electron band, we find for the length of the final wave vector inside the solid,

$$k = [(2m/\hbar^2)(\hbar\omega + W - E_b)]^{1/2},$$

where W is the position of the bottom of the band (with respect to E_F), called the inner potential. We will approximate W by the energy of the muffin-tin zero of the band-structure calculation: $W = 8.4$ eV. The perpendicular component of the wave vector (in the repeated-zone scheme) is now found to be

$$k_{\perp} = (k^2 - k_{\parallel}^2)^{1/2}.$$

However, k_{\perp} is not completely conserved, since during the transport to the surface the photoelectron can suffer several losses. This results in a loss of information on the perpendicular wave vector as well as a broadening of the photoemission peak. If k_{\perp} is completely undetermined, one simply measures the one-dimensional density of states along k_{\perp} at a given \vec{k}_{\parallel} (indirect-transition model).

In Figs. 10–12 we show the measured peak positions (dots) with their widths (bars) versus \vec{k}_{\parallel} . The calculated bands are also shown for \vec{k} in the ΓMK (solid curves) and ALH planes (dashed curves). We will compare the experimental “two-dimensional” band structure with the theoretical bands in both planes, because k_{\perp} is not known accurately and also because we have to average in some way over k_{\perp} . In addition to the HeII data of Figs. 8 and 11, we also measured some spectra at higher polar angles. If these data are folded back into the first Brillouin zone, they are the same as the data obtained directly in the first Brillouin zone. In Fig. 13 we plot the peak positions measured along a circle in the (two-dimensional) Brillouin zone, obtained by varying φ at a fixed θ (equal to 30°). These are compared with the theoretical band structure along KM (HL) because these points are approximately the same as those on the circle—within the experimental angular resolution. In Fig. 14 the peak positions are plotted versus k_{\perp} along high-symmetry directions, along with the theoretical bands.

Now we will examine the experimental band structure in some detail. At $k_{\parallel} = 0$, a peak in the HeI spectrum is seen at 4.3 eV, which extends between the bonding $\text{Te } 5p_z$ -derived bands Γ_1^+ and A_1^+ . Such a broad peak is expected if the mean free path λ is somewhat larger than the lattice constant c . Its position is in good agreement with theory for the calculated k_{\perp} (Fig. 14). At a higher polar angle the effective mean free path, which is about $\lambda \cos\theta$, is smaller, and we can expect to measure the one-dimensional density of states $(\partial E/\partial k_z)^{-1}$. As seen in Fig. 3 the density of states is large at the bottom of the band along ΓA , in agreement with the measured peak positions for $\vec{k}_{\parallel} \approx 2\Gamma M$ [Fig. 10(a)]. For $\hbar\omega = 45$ eV, a weak, broad peak is seen for which k_{\perp} is not conserved. The differ-

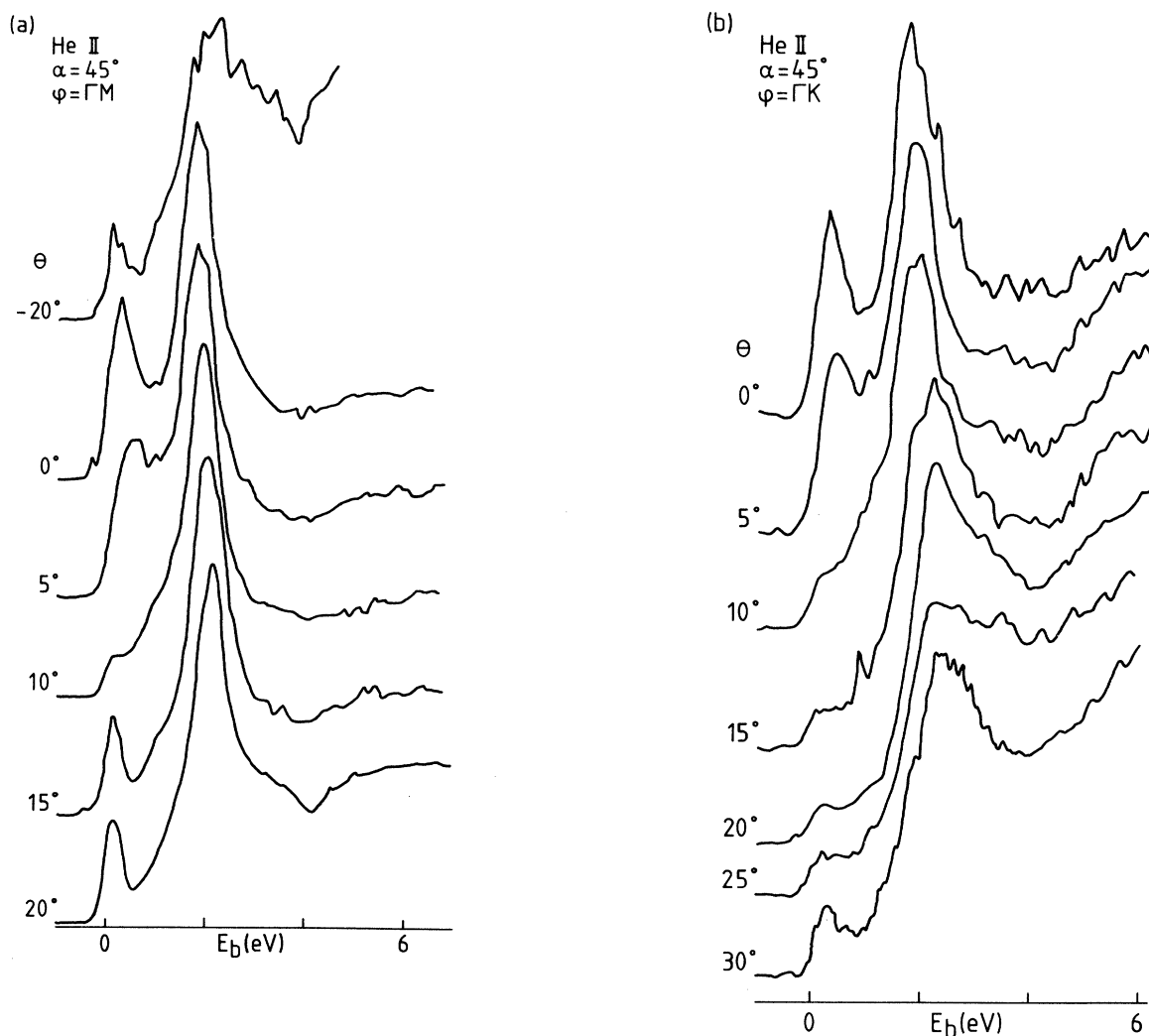


FIG. 8. He II photoelectron spectra of TiTe_2 for various emission angles θ , with $\alpha = 45^\circ$. (a) Emission in the ΓMA plane. (b) Emission in the ΓKA plane.

ence in peak positions for M and M' (Fig. 13) may be due to a different surface band structure in the two directions, arising from different surface potential gradients.

The calculated antibonding $\text{Te } 5p_z$ -derived band extends from 0 to 3.3 eV along ΓA . The broad peak at 1 eV is the best assignment for this band, as its maximum is in agreement with the calculated position along k_1 (Fig. 14). The flat band observed around 2 eV in all spectra is in good agreement with the calculated band, which, in addition to $\text{Te } 5p$, has a large amount of $\text{Ti } 3d$ mixed in. Near Γ (A) the experimental band is split. This may be due to spin-orbit coupling, which causes the Γ_3^+ band to split into Γ_{45}^+ and Γ_6^+ bands. Near M (L) the experimental points at about 3 eV seem to follow the calculated band along AL . The peak at 1 eV at M (L) is probably the $\text{Te } 5p_y$ -derived L_1^- state, which, because of relativistic effects, is "repelled" by L_2^- .

Along ΓK (AH), two bands with a large dispersion, which intersect the Fermi level near Γ (A), can be dis-

tinguished. They are in good agreement with the theoretical bands. Along ΓM (AL) the agreement is good for at least one of the bands which intersect E_F . We conclude from these measurements that TiTe_2 probably has two hole surfaces around Γ (A) with Fermi energies of a few tenths of an electron volt.

According to the band-structure calculations we expect electron surfaces around L . However, experimentally, a sharp peak is observed just below E_F in the entire Brillouin zone. It is not possible, of course, that there are so many electrons present that the $\text{Ti } 3d$ -derived band is completely occupied. Thus we have to assume that this emission is due to a small number of electrons, but also that \vec{k} is not a good quantum number for these electrons. The intensity of the peak just below E_F is the largest near M (L), and it has reached about half its maximum for $k_{||}$ values where the theoretical bands intersect the Fermi level (see Fig. 16). Both experimentally and theoretically we find a Fermi energy of about 0.2 eV for the

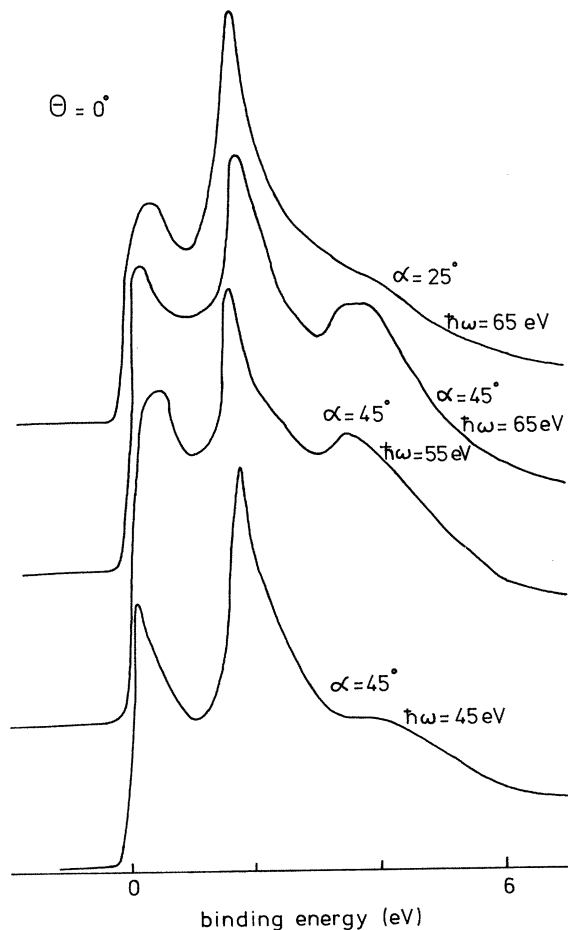


FIG. 9. Photoelectron spectra of TiTe_2 excited with synchrotron radiation of various energies and α 's at $\theta=0^\circ$.

Ti $3d$ -derived band. Thus, at least in the region in reciprocal-lattice space with the largest density of Ti $3d$ electrons, theory and experiment are compatible.

B. Intensities for photoemission from TiTe_2

In Fig. 15 we show the measured intensities as a function of angle of incidence α for He I radiation. As a measure for the intensities we took the peak height normalized to that of the peak at 2 eV. We must remark that the intensities are difficult to determine exactly, as they are easily changed by contaminations of the sample. Moreover, some peaks overlap, and thus at most, some trends can be seen in the intensity pattern.

Theoretical intensities were obtained by a method analogous to that used by Shevchik.²⁵ The initial state is considered to be a LCAO, whereas for the final state an APW is taken. We assume that at the given kinetic energy several waves exist, from which we can form an APW corresponding to one type of atom. Furthermore, only transitions within the muffin-tin sphere around each atom are considered. We assume that the matrix element for such a transition is equal to that for the free atom. These matrix elements can be calculated, as indicated by Gold-

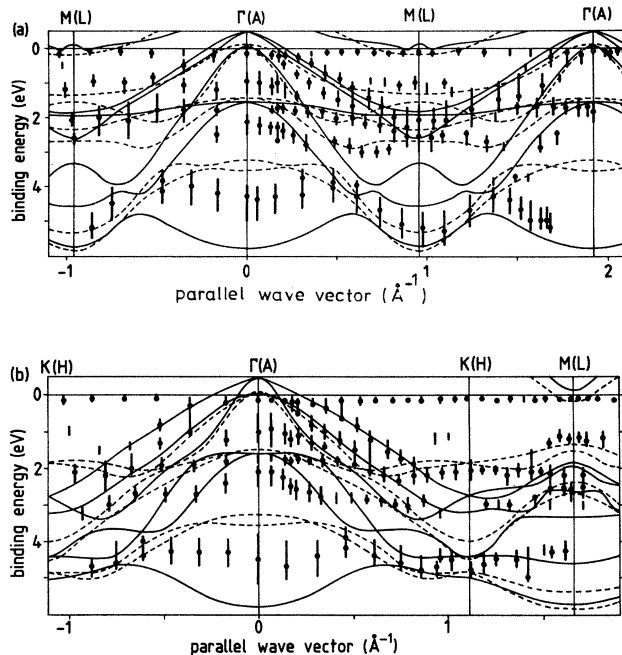


FIG. 10. Band structure $E(\vec{k}_{\parallel})$ measured for TiTe_2 with He I radiation and $\alpha=45^\circ$. Peak positions (dots) and widths at half height (bars) are plotted as a function of parallel wave vector in the repeated-zone scheme. Bars without dots indicate weak shoulders. Furthermore, the theoretical bands from Fig. 3 are shown for $k=0$ (solid curves) and $k_{\perp}=\pi/c$ (dashed curves). (a) Band structure along ΓM (AL). (b) Band structure along ΓKM (AHL).

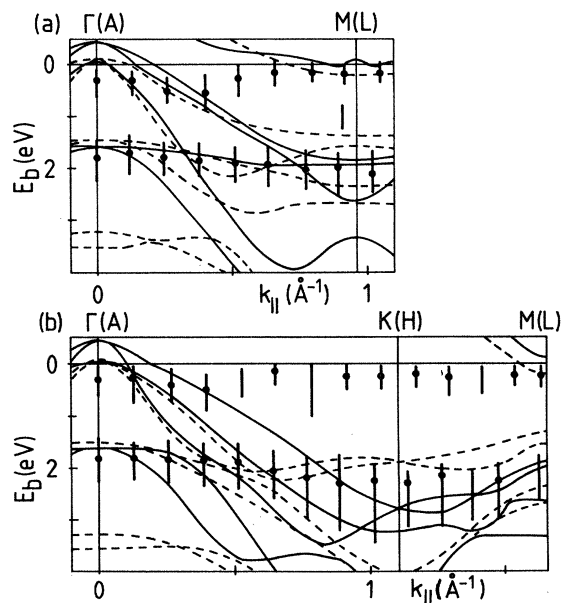


FIG. 11. Same as Fig. 10 for the measurements with He II radiation.

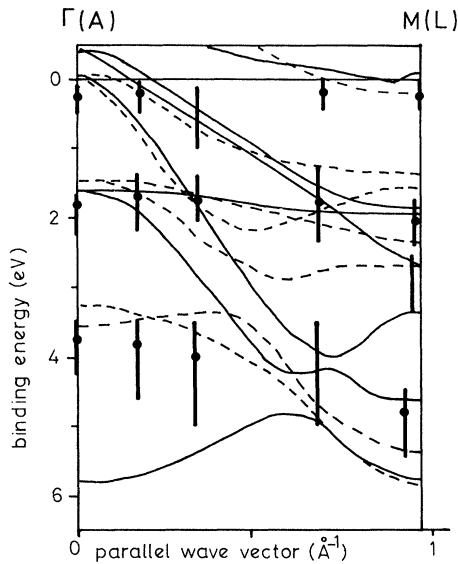


FIG. 12. Band structure $E(\vec{k}_{\parallel})$ for TiTe_2 measured with synchrotron radiation with $\hbar\omega = 65$ eV ($\alpha = 45^\circ$). Peak positions are indicated by dots and the width at half height is indicated by bars. The theoretical bands (Fig. 3) are shown for $k_{\perp} = 0$ (solid curves) and $k_{\perp} = \pi/c$ (dashed curves).

berg,²⁶ who calculated the necessary radial matrix elements and phase shifts for 21 elements. Those for Ti and Te were not calculated, and we use those for Ni and Sb instead. The required emission angle in the crystal of $\theta_f = \arcsin(k_{\parallel}/k)$. For unpolarized light the intensities are averaged over all values of the polarization vector. We only considered emission from \vec{k} points of high symmetry. For the initial-state coefficients we used those calculated for CrSe_2 (see Sec. IV).

The band at 2 eV contains both Te p and Ti d , but no p_z and d_{z^2} . We calculated that the intensity of this peak

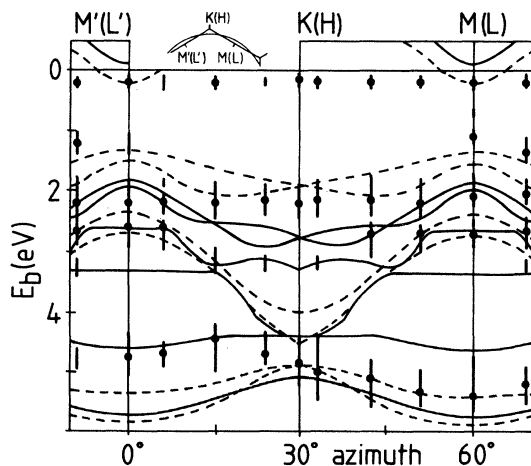


FIG. 13. Peak positions measured with HeI radiation at $\alpha = 45^\circ$ for $\theta = 30^\circ$ as a function of azimuth φ . The corresponding k_{\parallel} values lie on a circle in the Brillouin zone (see inset). The band structure calculated along KM (solid lines) and HL (dashed lines) is shown for comparison.

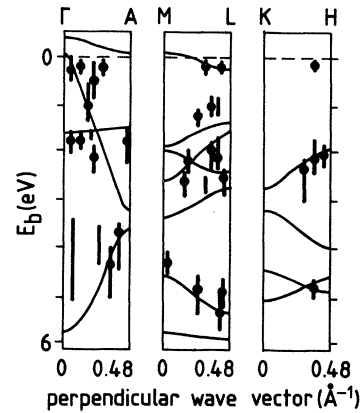


FIG. 14. Theoretical and experimental band structure (calculated with a free-electron dispersion for the final state) as a function of perpendicular wave vector k_{\perp} . Data for different directions and photon energies are assembled.

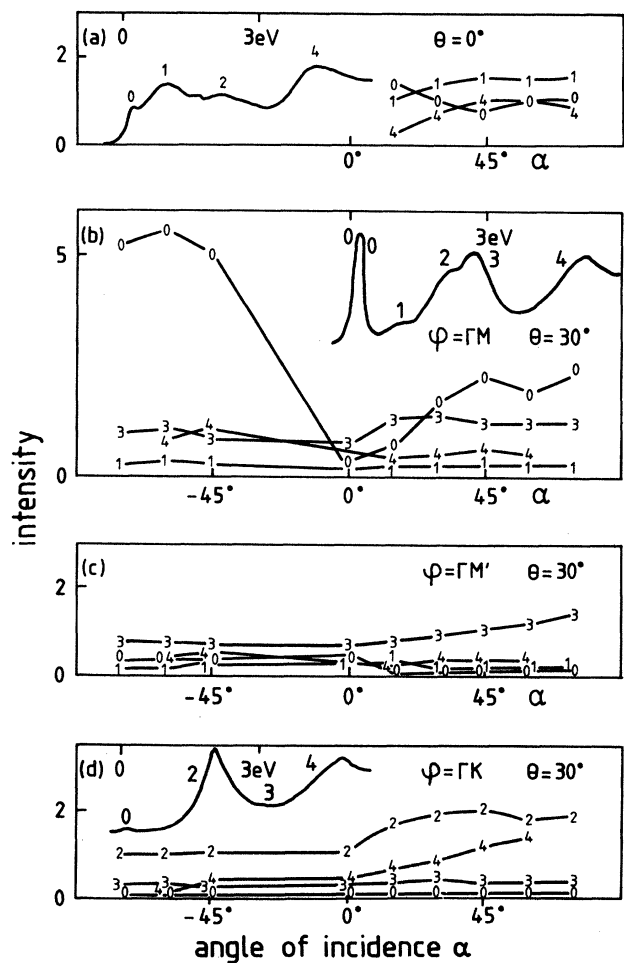


FIG. 15. Measured intensities (normalized at peak 2) versus angle of incidence α for HeI radiation. The peaks are numbered as shown.

is nearly independent of α , and thus it is reasonable to normalize the intensities of all other peaks to this peak. If our assignment is correct, the peaks at 1 and 4.5 eV at normal emission are mainly p_z . They are expected to grow with α , which is indeed seen.

Next, we consider emission for $\vec{k}_{\parallel} = k_{\Gamma M}$ (which we take as the x axis). The peak at 2 eV, to which we normalized the other peaks, is mainly Te p_y . The peak at 1 eV, remaining constant with varying α , can also be assigned as Te p_y -derived, in agreement with its assignment as a L_1^- state. The peak at 2.7 eV (peak 3) is stronger for positive than for negative α , in qualitative agreement with the intensity calculated for the mainly Te p_z -derived L_1^+ state at 2.7 eV. The peak at about 5 eV is weak, as calculated for the Te p_x -derived states M_1^+ and M_2^- .

For the peak just below E_F , good agreement between theory and experiment is not obtained. According to the band-structure calculation, we expect emission just below E_F from electrons in the L_1^+ state which is a mixture of Te p_z , Ti d_{z^2} , and Ti d_{xz} . The intensities calculated for positive and negative α are different, but the experimental pattern was not reproduced.

A complication in the calculations of the intensity is that at the boundary of the Brillouin zone we have to take, for the final state, a symmetrized combination of APW's with different \vec{G} 's instead of a single APW. This implies that in the ΓM and $\Gamma M'$ directions the same combination of APW's has to be taken, and thus the intensities have to be the same. We note that this fact seems not to have been realized by Shevchik and Liebowitz,²⁵ as they used a single APW for all wave vectors.

Experimentally, different intensities are observed for the ΓM and $\Gamma M'$ directions. As a function of azimuth φ , the intensities show a threefold symmetry, even at the border of the Brillouin zone [Fig. 16(c)]. We now discuss the mechanism which may be responsible for the different intensities of the peak just below E_F for $\vec{k}_{\parallel} = k_{\Gamma M}$ and $k_{\Gamma M'}$. In real space, a photoelectron originating from a Ti atom in the uppermost sandwich, emitted in the $\Gamma M'$ direction, encounters an anion, whereas in the ΓM direction it does not. It is possible that because of a sort of "shadowing effect,"²⁷ which for these low-energy electrons is better described as photoelectron diffraction,²⁸ the photoelectron in the $\Gamma M'$ direction does not come out of the solid. For HeII radiation no difference is seen between ΓM and $\Gamma M'$ (Fig. 8). A smaller difference is expected because the diffraction is less now that the electron is emitted under a smaller angle.

In the ΓK direction the peaks at 2 and 5 eV both grow with α . This can be explained if they originate from p_z orbitals. Indeed, the peak at 2 eV is mainly Te p_z , whereas one of the H_3 states has some Te p_z mixed in.

According to Goldberg's tables,²⁶ at higher photon energies emission from anion p bands decreases with respect to the metal d emission. This is indeed seen for the peak at 4 eV when going from HeI to HeII radiation. However, at higher photon energies this trend reverses (Fig. 9), perhaps because at higher energies more final states are attainable. It is also possible that better results are obtained if the proper matrix elements for Ti and Te (in-

stead of Ni and Sb) are used.

The peak at 2 eV has a large amount of Ti d mixed in and is seen in all spectra, as expected. From Fig. 9 ($\hbar\omega = 65$ eV) we see that the Te p_z -derived peak at 4 eV decreases strongly with decreasing α at normal emission. The peak just below E_F decreases only slightly. With decreasing α , and at $\hbar\omega = 21.2$ eV (Fig. 15), the intensity of this peak even increases. This indicates that, in this state, d_{z^2} (or p_z) as well as p_x is mixed in.

C. The localized state just below E_F

In Fig. 16 we plot the intensity of the peak near the Fermi level as a function of \vec{k}_{\parallel} . This peak is seen at all emission angles, but its intensity is the largest for \vec{k} values where a band is seen in the theoretical band structure. We see that in TiTe_2 , the peak is intense for $k_{\parallel} \approx 0.2 \text{ \AA}^{-1}$, probably because of overlap with the Te $5p$ -derived bands which intersect E_F at that value of \vec{k} (cf. Figs. 10 and 11). An appreciable intensity is also seen at Γ .

A narrow emission peak near E_F is observed in nearly all layered compounds: TaS_2 and TaSe_2 ,²⁷ VSe_2 ,²⁹ and TiSe_2 .⁹ Schärli *et al.*⁵ also observed a peak in TiS_2 near the Fermi level with k values over the entire Brillouin zone. The intensity of this peak increased in going from excitation with HeI to HeII radiation, indicating a strong Ti $3d$ character. The intensity increases with increasing vanadium content in $\text{Ti}_{1-x}\text{V}_x\text{S}_2$ crystals. As each V atom provides an extra electron, this is also consistent with an assignment to emission from Ti $3d$ states. Schärli *et al.*⁵

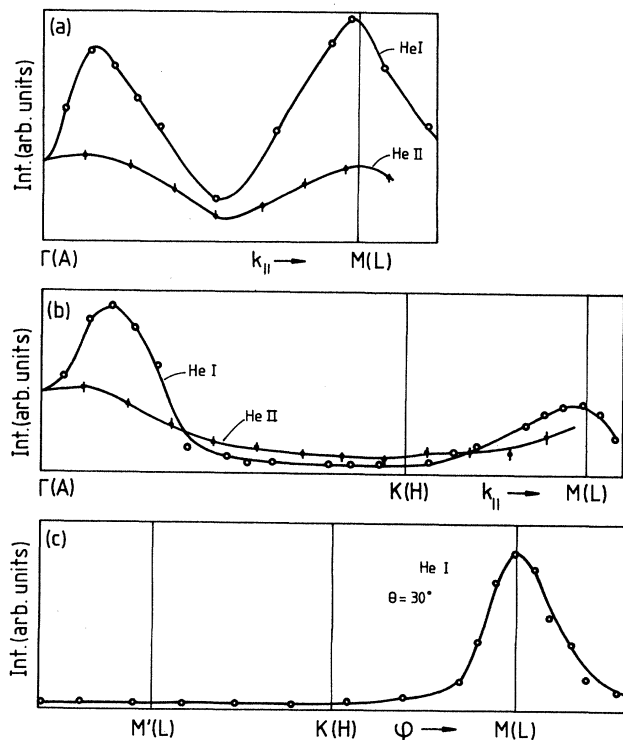


FIG. 16. Intensity versus \vec{k}_{\parallel} for the peak just below E_F ($\alpha = 45^\circ$): (a) along ΓM (AL), (b) along ΓK (AH), and (c) along a circle in the Brillouin zone (at $\theta = 30^\circ$; see inset of Fig. 11).

ascribed the peak near E_F to a localized impurity band just below E_F arising either from Ti excess and/or V impurities. They also determined the intensity of the peak near E_F as a function of polar angle. Near point M or L an enhancement of the relative intensity by a factor of 4–5 with respect to normal emission was found. The authors ascribed this to a superposition of emission of electrons from a dispersionless impurity band and electrons from the conduction band near point L .

It is possible that the narrow peak near E_F in TiTe_2 is also due to emission from a narrow impurity band, due, in turn, to excess Ti atoms. However, we want to point out an alternative explanation for the observed narrow peak near E_F . It is possible that there exists an interaction, for instance, an electron-phonon interaction or electronic polarization, which mixes the one-particle states. From Fig. 3 we see that the conduction-band states near L (M) and Γ (A) are fairly close in energy, whereas K (H) has a much higher energy. Therefore we expect a strong mixing of L (M) with Γ (A), but not with K (H) states. This is in agreement with the region in \vec{k} space where strong emission is observed. Te $5p$ states near Γ (A) may also contribute.

If states with different \vec{k} values are mixed, it is possible to obtain a localized (quasi)particle in real space. The states which are mixed have a spread Δk , and the electron can be localized in a region in direct space with a dimension of the order $(\Delta k)^{-1}$. An appropriate name for such a dressed electron, which has a certain spread in both direct and reciprocal-lattice space, may be “blur.”³⁰ If polarization of the environment is responsible for the mixing of states, the quasiparticle is a (electronic or vibronic) polaron. Of course, the corresponding polaron band has the full crystal symmetry, and the wave vector \vec{k} of the polaron is a good quantum number. However, if an electron is photoemitted from a state of the polaron band, the polarization cloud which remains behind can have an arbitrary \vec{k} . It is interesting that, in principle, with ARUPS one can measure the internal \vec{k} distribution of the particle. Neglecting matrix-element effects, the Fourier transform of the spatial distribution of the more or less localized quasiparticle is obtained directly with ARUPS.

We have no additional information on the nature of the interactions which produce the localization of Ti $3d$ electrons in TiTe_2 . However, we remark that the dispersionless narrow d band is observed in several highly polarizable layered compounds with d electrons. The very large temperature-independent paramagnetic susceptibility observed in some of these compounds (TiTe_2 , VSe_2 , and CrSe_2) indicates that the d electrons are itinerant but not far from forming localized magnetic moments. It is unlikely that in compounds with a high concentration of d electrons (VSe_2 , TaS_2 , TaSe_2 , and CrSe_2) the localization of so many electrons could be produced by a relatively small number of impurity atoms.

VI. MAGNETIC SUSCEPTIBILITY AND ELECTRICAL TRANSPORT MEASUREMENTS

In Figs. 17 and 20 we show the magnetic susceptibility χ and the thermoelectric power α of polycrystalline sam-

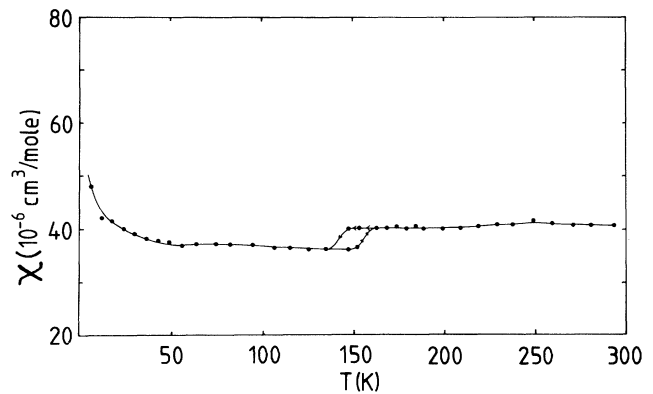


FIG. 17. Magnetic susceptibility of TiTe_2 (nonoriented) crystals vs temperature; $H = 8.76$ kOe.

ples of TiTe_2 . In Figs. 18 and 19 we show the in-plane resistivity ρ and Hall coefficient R_H (with $\vec{H} \parallel c$ axis) of a single-crystal platelet of TiTe_2 . We remark that at $T < 125$ K, R_H is positive and α is negative, indicating that TiTe_2 is a semimetal with overlapping valence and conduction bands.

For an analysis of the transport properties we first estimate the concentrations of electrons in the conduction band (n) and holes in the valence band (p). According to the band-structure calculations in stoichiometric TiTe_2 , $n_0 = p_0 = 0.052$ per unit cell, or $n_0 = p_0 = 6.5 \times 10^{20} \text{ cm}^{-3}$. In our considerations we will not take into account that the holes are distributed over three different valence bands. Therefore the properties of the holes (mobility, etc.) to be obtained below refer to average values.

The crystals we studied contained an excess of approximately 1 at. % Ti. The excess Ti atoms occupy interstitial sites in the van der Waals gap, and each Ti atom is expected to donate four electrons to the conduction band. Therefore, in our crystals, carrier concentrations are $p = 0.052$ and $n = 0.092$ per unit cell, or $p = 6.5 \times 10^{20} \text{ cm}^{-3}$ and $n = 11.5 \times 10^{20} \text{ cm}^{-3}$.

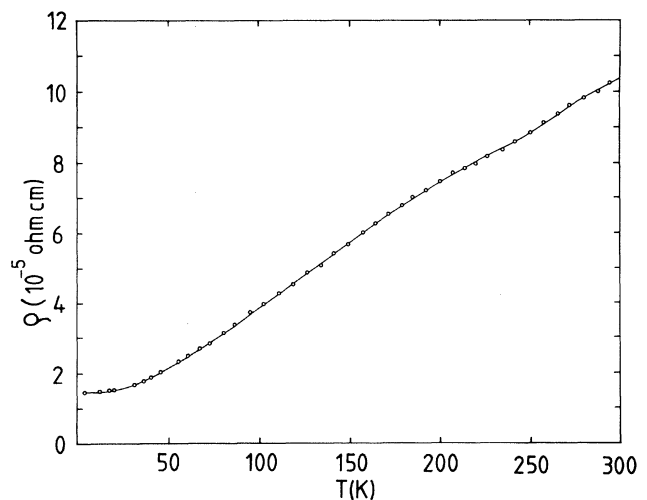


FIG. 18. In-plane resistivity of TiTe_2 crystal plate vs temperature.

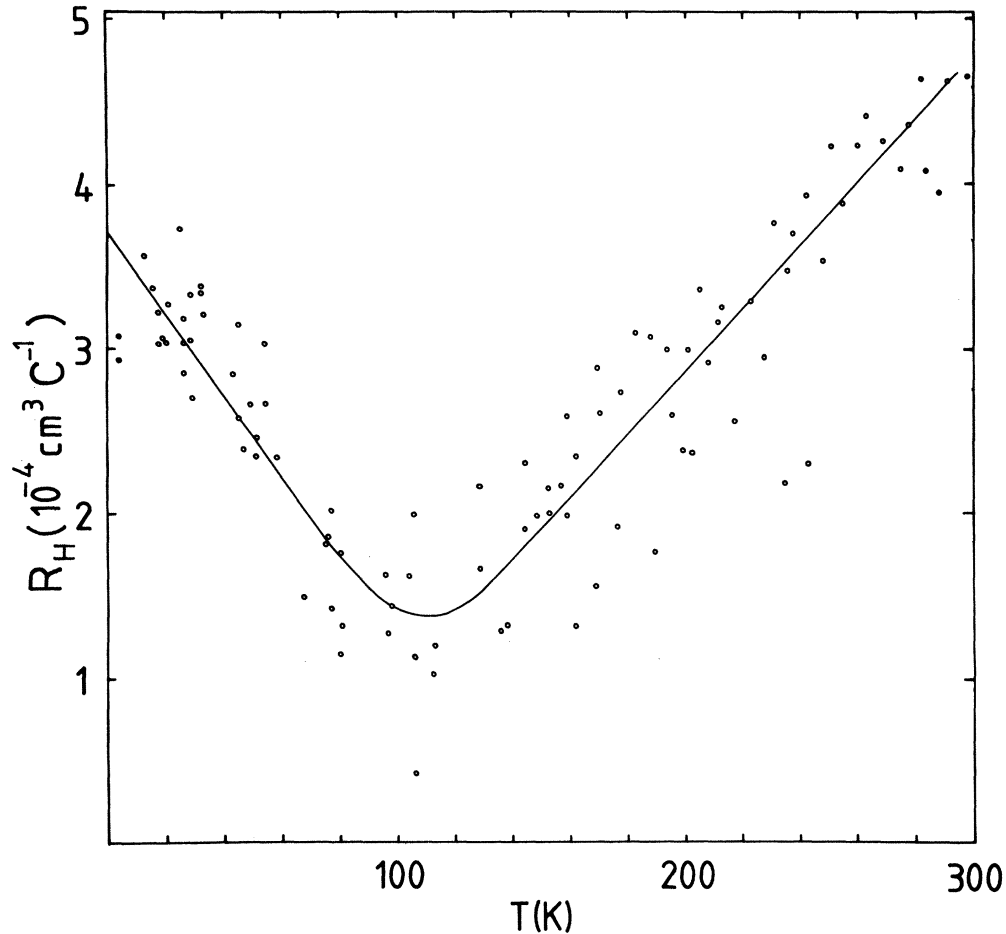


FIG. 19. Hall effect of TiTe_2 crystal plate vs temperature.

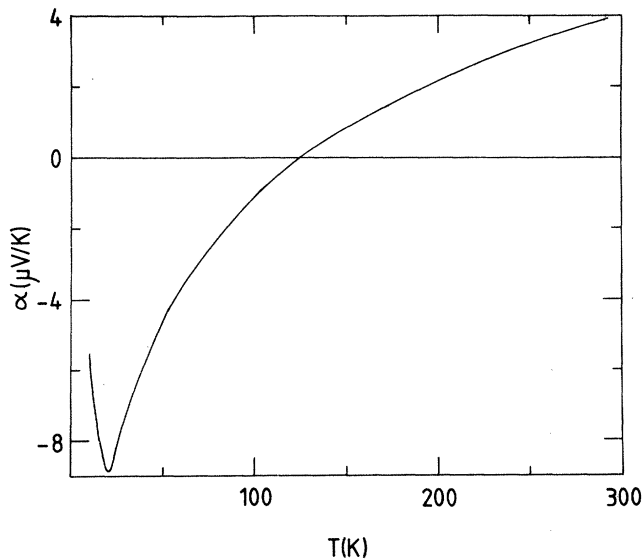


FIG. 20. Thermoelectric power of TiTe_2 powder vs temperature.

We analyze the Hall and resistivity data at 300 K with a simple two-carrier model, with

$$\rho^{-1} = \sigma_n + \sigma_p, \quad \sigma_n = ne\mu_n, \quad \sigma_p = pe\mu_p,$$

$$R_H = \frac{1}{e} \frac{p\mu_p^2 - n\mu_n^2}{(p\mu_p + n\mu_n)^2},$$

where μ_n and μ_p are the mobilities of electrons and holes, respectively.

From the values of n and p and the measured Hall coefficient, it is possible to calculate the ratio of electron and hole mobilities: we obtain, at 300 K, $\mu_p/\mu_n = 1.52$. Combining this result with the values of ρ , we find, for the mobilities at 300 K, the values $\mu_p = 43 \text{ cm}^2/\text{V sec}$ and $\mu_n = 28 \text{ cm}^2/\text{V sec}$.

From this analysis we find that the Hall effect consists of contributions of electrons and holes which nearly compensate for each other. Therefore the Hall effect will be sensitive to small variations of the carrier concentrations (due to a change of stoichiometry) or the mobility ratio (due to a change of temperature). The Hall effect, and also the thermoelectric power, show a very pronounced temperature dependence; the thermoelectric power

changes sign at 125 K. These changes are due to changes of charge carrier concentrations (and mobilities), and are related to the phase transition at 150 K. This phase transition is probably due to the same type of interactions which produce static charge-density waves in compounds such as TiSe_2 .^{1,2}

In a recent paper, Koike *et al.*³¹ also reported transport measurements of TiTe_2 . These authors found a Hall effect with about the same magnitude, sign, and temperature dependence as obtained from our samples. Koike's samples are probably closer to stoichiometry due to the lower temperature at which the crystals were grown. The better stoichiometry of Koike's samples corresponds to the observed lower residual resistivity at 5 K due to impurity scattering.

Koike *et al.*³¹ observed a logarithmic temperature dependence of the resistivity between 0.5 and 5 K. From magnetoresistance measurements it was concluded that the logarithmic temperature dependence of ρ is not due to a Kondo effect, but to a two-dimensional (2D) Anderson localization. In order to be able to interpret the data the authors suggested two types of charge carriers in TiTe_2 , i.e., 3D hole pockets at point Γ , and 2D electrons along LM lines, in good agreement with our results. The 2D electrons would then undergo the Anderson localization at low temperature.

The thermoelectric power of metals can be written as

$$\alpha = -\frac{\pi^2 k^2 T}{3e} \left[\frac{\partial \ln \Lambda}{\partial E} + \frac{\partial \ln S}{\partial E} \right]_{E=E_F},$$

where Λ is the mean free path of the electrons, S is the area of the Fermi surface, and E is the electron energy.³² For spherical energy bands, electrons give a negative, and holes a positive contribution to α . However, the thermoelectric power of a metal with a complicated Fermi surface such as that of TiTe_2 (see Fig. 5) is difficult to interpret quantitatively. One expects positive contributions for the hole surfaces (sheets 6, 7, and 8) for which the area S of the Fermi surface decreases with increasing energy E . Generally, one expects a negative contribution to α from electrons in the conduction band, because for these electrons, S increases with E . However, the electron Fermi surface (sheet 9 in Fig. 5) has a complicated shape and also has holelike parts for which $dS/dE < 0$. Electrons in these parts of the conduction band will give a positive contribution to α . This is probably the reason that α is positive in our crystals, although $n > p$.

Finally, we discuss the magnetic susceptibility. If we correct the observed χ with a diamagnetic contribution of $-145 \times 10^{-6} \text{ cm}^3/\text{mol}$, we obtain a value of $\chi_p = +183 \times 10^{-6} \text{ cm}^3/\text{mol}$, which we attribute to the Pauli paramagnetic susceptibility of the charge carriers. The value of χ_p is much larger than the bare value of $\frac{2}{3} \mu_B^2 N(E_F) = 27 \times 10^{-6} \text{ cm}^3/\text{mol}$, calculated from the density of states $N(E_F) = 1.26 \text{ states/eV unit cell}$ obtained from the band-structure calculation (taking into account a small increase of E_F in $\text{Ti}_{1.01}\text{Te}_2$ due to the extra electrons from 1 at. % excess Ti). We attribute the increased susceptibility to the exchange enhancement γ , so that the Pauli paramagnetic susceptibility is given by

$$\chi_p = \frac{2}{3} \gamma \mu_B^2 N(E_F) \quad \text{with } \gamma = \frac{1}{1 - E_x N(E_F)}.$$

From the observed value of χ_p and the calculated value of $N(E_F)$ we obtain a value $\gamma = 7$, which corresponds to an exchange energy $E_x = 0.7 \text{ eV}$. We note that a large exchange enhancement is also necessary to explain the observed susceptibilities of VSe_2 and CrSe_2 . An appreciable exchange enhancement is indeed expected for transition-metal $3d$ electrons.

The magnetic susceptibility shows an abrupt change and a hysteresis at 150 K. Similar effects were observed at 150 K in the specific heat. These effects are due to a first-order phase transition in TiTe_2 , which is probably of the charge-density-wave type. The lattice distortion corresponding to this phase transition must be small, as no change in crystal structure or lattice parameters could be detected at 150 K.

VII. CONCLUSIONS AND SUGGESTIONS

We have seen that it is possible to extract interesting information on the band structure of the semimetallic compound TiTe_2 from angular-resolved photoelectron spectra. The measurements are in good agreement with a band structure calculated using the APW method. Attention was also given to the intensities in the photoemission spectra. Although these are difficult to treat both experimentally and theoretically, the assignment of peaks can be facilitated if the intensities are also considered.

An analysis showed the transport properties can be explained quite well with a simple two-carrier model. The charge carrier concentrations for TiTe_2 were deduced from band-structure calculations and from the Ti excess of 1 at. % found by chemical analysis. Neither of these data are expected to be very precise, and therefore the values of n , p , μ_n , and μ_p are not expected to be very accurate. However, the analysis shows that the transport data are consistent with the band-structure calculations.

A remarkable phenomenon in the angular-resolved spectra of TiTe_2 (and similar compounds) is the occurrence of states, just below the Fermi level, which cannot be characterized by a single wave vector. These states are like a "blur" with a certain spread in direct and in reciprocal-lattice space. This localization could be due to the presence of impurities in the crystal. Another possibility is a lowering in energy of a localized electron, due to polarization of the environment, analogous to broken-orbital-symmetry calculations for molecular systems.³³ The original band states will be mixed to form a wave packet for the localized electron. The energy of the localized particle can be expressed in terms of the energies of these states, obtained from the band structure, and in terms of the polarizability of the environment. In this way, a decomposition is obtained of the localized state in different \vec{k} states which corresponds to the measured photoemission distribution.

The dispersionless band near E_F was observed in photoemission, which is a surface-sensitive technique, and it is possible that the observed localization only occurs for Ti

3d electrons at the surface. However, for a surface state we expect appreciable changes with photon energy or a contaminated surface, which we did not observe.

Our conclusion is that the observation of the dispersionless electron band just below E_F , the strong exchange enhancement of the magnetic susceptibility, and the low-temperature resistivity data (Anderson localization) strongly indicate an anomalous and (nearly) localized behavior of the conduction electrons in TiTe_2 .

Finally, we suggest a relation between the proposed model of an (electronic) polaron in TiTe_2 and the charge-density-wave instabilities of layer compounds as in TiSe_2 .³⁴ The large intensity of the "blur" at points Γ and L suggests that these states are in some way coupled. Such a coupling is known to cause the instability in TiSe_2 . The nature of the coupling is not known, but both electron-phonon and excitonic interactions must be involved.³⁵ In TiTe_2 , the partial localization of a conduction electron in an electronic polaron will induce shifts of the Ti atoms leading to a composite electronic-vibronic

polaron ("blur"). Such a structure is similar locally to the distortions observed in TiSe_2 below the phase transition. Above the phase transition such distortions will still be present but they will be dynamic in nature ("blur"), so that no long-range order exists. In TiTe_2 , the phase transition at 150 K could correspond to an ordering of the "blurs," although this was not detectable using x-ray diffraction.

ACKNOWLEDGMENTS

We would like to thank E. Tosatti for helpful discussions. This investigation was supported by the Netherlands Foundation for Chemical Research [Scheikundig Onderzoek Nederland (SON)] with financial aid from the Netherlands Organization for the Advancement of Pure Research (Nederlandse Organisatie voor Zuiver-Wetenschappelijk Onderzoek) (ZWO), in conjunction with the collaborative agreement between ZWO and the United Kingdom Science and Engineering Research Council on the use of synchrotron radiation.

- ¹J. A. Wilson, F. J. Di Salvo, and S. Mahajan, *Adv. Phys.* **24**, 117 (1975).
- ²J. A. Wilson, *Phys. Status Solidi B* **86**, 11 (1978), and references therein.
- ³C. H. Chen, W. Fabian, F. C. Brown, K. C. Woo, B. Davies, and B. de Long, *Phys. Rev. B* **21**, 615 (1980).
- ⁴J. J. Barry, H. P. Hughes, P. C. Klipstein, and R. H. Friend (unpublished).
- ⁵M. Schärli, J. Brunner, H. P. Vaterhaus, and F. Lévy, *J. Phys. C* **16**, 1527 (1983).
- ⁶F. J. DiSalvo, D. E. Moncton, and J. V. Waszczak, *Phys. Rev. B* **14**, 4321 (1976).
- ⁷R. Z. Bachrach, M. Skibowski, and F. C. Brown, *Phys. Rev. Lett.* **37**, 40 (1976).
- ⁸W. Drube, G. Karschnik, M. Skibowski, R. Thies, and K. Völkert, in *Proceedings of the 15th International Conference on the Physics of Semiconductors, Kyoto, 1980*, edited by S. Tanaka and Y. Toyozawa [*J. Phys. Soc. Jpn. Suppl. A* **49**, (1980)], p. 137.
- ⁹M. M. Traum, G. Margaritondo, N. V. Smith, J. E. Rowe, and F. J. Di Salvo, *Phys. Rev. B* **17**, 1836 (1978).
- ¹⁰G. Margaritondo, C. M. Bertoni, J. H. Weaver, F. Lévy, N. G. Stoffel, and A. D. Katnani, *Phys. Rev. B* **23**, 3765 (1981).
- ¹¹N. G. Stoffel, F. Lévy, C. M. Bertoni, and G. Margaritondo, *Solid State Commun.* **41**, 53 (1982).
- ¹²R. H. Friend, D. Jérôme, W. Y. Liang, J. C. Mikkelsen, and A. D. Yoffe, *J. Phys. C* **10**, L705 (1977).
- ¹³P. C. Klipstein and R. H. Friend, in *Europhysics Conference Abstracts*, edited by V. Heine (European Physical Society, Petit-Lancy 2, Switzerland, 1982), Vol. 6A, p. 351.
- ¹⁴(a) A. Zunger and A. J. Freeman, *Phys. Rev. B* **16**, 906, (1977); (b) *Phys. Rev. B* **17**, 1839 (1978).
- ¹⁵Y. Arnaud and M. Chevreton, *J. Solid State Chem.* **39**, 230 (1981).
- ¹⁶G. A. Wieggers (unpublished).
- ¹⁷R. B. Murray and A. D. Yoffe, *J. Phys. C* **5**, 3038 (1972).
- ¹⁸D. W. Bullett, *J. Phys. C* **11**, 1501 (1978).
- ¹⁹H. W. Myron (unpublished).
- ²⁰H. W. Myron and F. M. Mueller, *Phys. Rev. B* **17**, 1828 (1978).
- ²¹H. W. Myron, *Physica* **99B**, 243 (1980).
- ²²A. Zunger and A. J. Freeman, *Phys. Rev. B* **19**, 6001 (1979).
- ²³G. D. Mahan, *Phys. Rev. B* **2**, 4334 (1970).
- ²⁴H. P. Hughes and W. Y. Liang, *J. Phys. C* **6**, 1684 (1973).
- ²⁵N. J. Shevchik and D. Liebowitz, *Phys. Rev. B* **18**, 1618 (1978).
- ²⁶S. M. Goldberg, C. S. Fadley, and S. Kono, *J. Electron. Spectrosc. Relat. Phenom.* **21**, 285 (1981).
- ²⁷N. V. Smith and M. M. Traum, *Phys. Rev. B* **11**, 2087 (1975); M. M. Traum and N. V. Smith, *Surf. Sci.* **53**, 121 (1975).
- ²⁸D. Norman and D. P. Woodruff, *Phys. Rev. B* **18**, 6789 (1978).
- ²⁹H. P. Hughes, C. Webb, and P. M. Williams, *J. Phys. C* **13**, 1125 (1980).
- ³⁰E. Tosatti (private communication).
- ³¹Y. Koike, M. Okamura, T. Nakanomyo, and T. Fukase, *J. Phys. Soc. Jpn.* **52**, 597 (1983).
- ³²J. Ziman, *Electrons and Phonons* (Oxford University Press, London, 1967).
- ³³P. S. Bagus and H. F. Schaffer III, *J. Chem. Phys.* **54**, 224 (1972); R. Broer and W. C. Nieuwpoort, *Chem. Phys.* **54**, 291 (1981).
- ³⁴F. J. DiSalvo, D. E. Moncton, and J. V. Waszczak, *Phys. Rev. B* **14**, 4321 (1976).
- ³⁵Y. Yoshida and K. Motizuki, *J. Phys. Soc. Jpn.* **49**, 898 (1980).